We are IntechOpen, the world's leading publisher of Open Access books Built by scientists, for scientists

6,900
Open access books available

185,000
International authors and editors

200M
Downloads

154
Countries delivered to

Our authors are among the

TOP 1%
most cited scientists

12.2%
Contributors from top 500 universities

BOOK CITATION INDEX
CLARIVATE ANALYTICS
INDEXED

WEB OF SCIENCE™

Selection of our books indexed in the Book Citation Index
in Web of Science™ Core Collection (BKCI)

Interested in publishing with us?
Contact book.department@intechopen.com

Numbers displayed above are based on latest data collected.
For more information visit www.intechopen.com

Improving Food Safety by Using One- and Two-Photon-Induced Fluorescence Spectroscopy for the Detection of Mycotoxins

Lien Smeesters, Wendy Meulebroeck and
Hugo Thienpont

Additional information is available at the end of the chapter

Abstract

The presence of mycotoxins in food products is a major worldwide problem. Nowadays, mycotoxins can only be detected by the use of sample-based chemical analyses. Therefore, we demonstrate the use of one- and two-photon-induced fluorescence spectroscopy for the non-destructive detection of mycotoxins in unprocessed food products. We first explain our optical set-up, which is able to measure the localized one- and two-photon-induced fluorescence spectra. Following, as a case study, the detection of aflatoxin in maize kernels is discussed. We present our research methodology, from the characterization of the fluorescence of pure aflatoxin, to the study of the one- and two- photon-induced fluorescence spectra of maize kernels and the development of an optical detection criterion. During both one- and two-photon-induced fluorescence processes, the fluorescence of the aflatoxin influences the intrinsic fluorescence of the maize. Based on the fluorescence spectrum between 400 and 550 nm, a detection criterion to sense the contaminated kernels is defined. Furthermore, we successfully monitored the localized contamination level on the kernel's surface, showing both contaminated kernels with a high contamination in a limited surface area (a few square millimetres) and kernels with a low contamination spread over a large surface area (up to 20 mm^2). Finally, the extensibility of our research methodology to other fluorescent mycotoxins is discussed.

Keywords: spectroscopy, fluorescence, two-photon-induced fluorescence, optical sensing, aflatoxin, multiphoton processes, spectrum analyses

1. Introduction

Fluorescence can be defined as the emission of electromagnetic radiation during the relaxation process of an excited electron that was excited from the ground state to a higher energetic state by the absorption of light. Fluorescence spectroscopy studies the fluorescence light emission as function of the wavelength. To date, fluorescence spectroscopy is already integrated in an extensive range of applications in, amongst others, the biochemical, medical and petrochemical industry [1–5]. In biology and chemistry, it facilitates the study of proteins and the tracking of biochemical reactions. In the medical industry, it is used to follow smart drug delivery systems that map the drug interaction with diseased tissue, while in the petroleum industry, it enables to characterize crude oils during refining processes.

Considering food applications, fluorescence spectroscopy has currently been demonstrated for the screening of products on basis of their chlorophyll concentration [6–8]. Particularly, the detection of foreign objects in food streams has been presented, by comparing the fluorescence spectra of the food products and the foreign objects. For example, when considering a mixture of green glasses and peas, a distinction can be made on basis of the chlorophyll fluorescence intensity, since the peas emit strong fluorescence signals while the glasses emit no fluorescence. In addition, also a distinction between peas, garden beans and sprouts has been demonstrated by evaluating the shape of the chlorophyll fluorescence spectrum [6]. However, toxic contaminants in food and feed products can hardly be optically detected due to the presence of large background fluorescent signals emitted by natural food constituents, like proteins, and the localized presence of the toxins. The current published fluorescence measurements only allow the identification of mycotoxins in homogeneous liquids, like beer or wine, in which no or very low background fluorescent elements are present [9, 10]. Therefore, we investigate the use of fluorescence spectroscopy for the detection of mycotoxins in unprocessed, solid food products.

Mycotoxins are secondary metabolites of toxic fungi, produced by various moulds on a wide range of food products, like nuts, maize, pistachios and peanuts [11]. Six types of mycotoxins are identified as major threats to food safety, of which we focus on the fluorescent mycotoxins, being aflatoxin, ochratoxin and zearalenone. Mycotoxins are observed under a diverse range of environments, both before and after the harvest [11]. Moreover, they appear both in the raw as processed products, since they cannot be destroyed during food processing, like cooking, freezing and roasting. The Food and Agriculture Organization (FAO) estimates that 25% of the world's food crops are affected by mycotoxin-producing fungi. The accumulation of mycotoxins in food and feed products represents a major threat to human and animal health, because they can induce cancer, liver diseases, immune-system suppression, mutagenicity and nervous disorders [9]. Therefore, to decrease the exposure to mycotoxins, international regulations were established [12, 13]. For example, for aflatoxins, the European Commission stated maximum allowed concentrations in the range between 2 and 15 ppb, depending on the commodity, while the USA food safety regulations included a maximum contamination level of 20 ppb for all food products. To fulfil these limitations, mycotoxins are nowadays detected by using time-consuming, sample-based chemical analyses, like liquid chromatography-dual mass spectrometry (LC-MS/MS). However, due to the localized presence of the toxin in the

food products and crops, these analyses often give a limited view on the degree of contamination, inducing a large amount of food waste, without entirely preventing the toxins to enter the food chain [11]. Consequently, to increase food safety, the development of a non-destructive detection methodology, which is able to identify the localized contamination on the food products, is indispensable.

We investigate the use of fluorescence spectroscopy, including one- and two-photon-induced fluorescence (OPIF and TPIF) spectroscopy, as a non-destructive, optical detection technique for the sensing of fluorescent mycotoxins. OPIF and TPIF are two types of fluorescent processes, both resulting in the emission of a fluorescent photon during the relaxation process of an excited electron, but with a different excitation process [14]. To generate an OPIF photon, only a single excitation photon needs to be absorbed, while during the generation of a TPIF photon, two excitation photons need to be absorbed simultaneously to excite the electron and generate the fluorescence signal (**Figure 1**). In the case of OPIF, the energy of the incident photon equals the energy difference between the electronic states, such that the electron obtains sufficient energy to bridge the energy gap between the ground state and the excited state (**Figure 1(a)**). Considering TPIF, the sum of the energies of the two incident photons must equal the bandgap energy (**Figure 1(b)**). The first incident photon excites the electron to a virtual state, which does not need to correspond to any electronic or vibrational energy eigenstate. The second incident photon excites the electron from the virtual state to its higher-energy excited state. Because for both OPIF and TPIF the electron is excited to the same energetic state, they give rise to the same fluorescence wavelengths, but with the use of another excitation wavelength. Generally, OPIF requires ultraviolet (UV) excitation wavelengths, while TPIF uses near-infrared (NIR) light. If the energy of the incident photons does not match with the bandgap, no fluorescence emission will occur. As a result, because the bandgap is a molecular specific property, fluorescence is known to be a selective process. In addition, because TPIF is a non-linear process that requires the simultaneous absorption of two photons instead of one, it is considered to be more selective than OPIF [10].
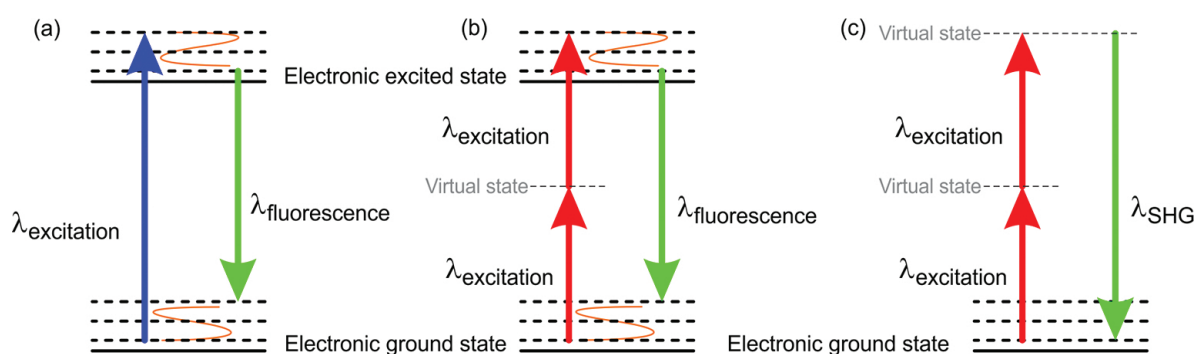

Figure 1. Jabloński diagram for (a) OPIF, in which the electron is excited by the absorption of a single incident photon; (b) TPIF, in which the electron is excited by the simultaneous absorption of two incident photons; (c) second harmonic generation, in which two incident photons recombine to a new photon with the double energy.

Two-photon excitation was first theoretically described by Mario Göppert-Mayer in 1931. However, two-photon fluorescence has only been experimentally demonstrated in the 1960s

by Kaiser and Garret when exciting an europium-doped crystal [15]. To date, two-photon fluorescence is mostly used in biomedical engineering, when studying living cells and tissue by using two-photon fluorescence microscopy [16–18]. Intuitively, we would expect that all fluorescent molecules, able to emit OPIF, generate a TPIF signal if they are excited with laser light with the double wavelength and a sufficiently high excitation power density. However, according to the quantum physics selection rules that describe the electron transitions in molecules, one- and two- photon absorption follow different selection rules [19]. More specifically, the occurrence of both OPIF and TPIF electronic transitions is only allowed in non-centrosymmetric molecules. When considering centrosymmetric molecules, the electron transition between the ground state and the excited state is allowed for either OPIF or TPIF. For these molecular structures, no TPIF signals can be observed if OPIF signals can be emitted.

Two-photon-induced fluorescence should not be confused with second-harmonic generation (SHG) (**Figure 1(c)**). SHG is generally defined as a non-linear optical process in which photons with the same energy interacting with a non-linear material are combined to generate new photons with the double energy and thus half the wavelength of the initial photons [20]. Considering the Jabłoński diagram for SHG, the two incident photons do not excite the electron but recombine to a new photon with an energy equal to the total energy of the two incident photons. Since no electron is excited, the process does not contain any information about the molecular structure of the products, making it unusable for the detection of toxins.

OPIF and TPIF spectroscopy are both considered as promising optical detection techniques. OPIF shows stronger fluorescence signals than TPIF, giving rise to a strong mycotoxin signal of the solid food products that enables the detection of low contamination levels. Particularly, the OPIF intensity increases linearly with the excitation power, while the TPIF intensity increases with the square of the excitation power. However, the TPIF process features a more selective excitation of the mycotoxins, which can reduce the influence of the background fluorescent signals emitted by the natural fluorescent substituents of the food products. Moreover, TPIF is obtained after excitation with NIR laser light that is more widely commer-cially available than the required UV laserlines used during OPIF. In addition, compact NIR lasers generally feature higher output powers than UV lasers, enhancing the fluorescence signal. When using UV light in an optical set-up, the optical mirrors and lenses need to be made from or coated with fused silica, resulting in a more expensive set-up than for NIR wavelengths.

In this chapter, we demonstrate the use of OPIF and TPIF as valuable tools for the non-destructive detection of mycotoxins. We first present our measurement configuration, able to study both OPIF and TPIF. Second, we discuss our measurement methodology, including the selection of the excitation wavelengths. Following, as a case study, we investigate the detection of aflatoxin B1 in individual maize kernels. This is because aflatoxin is considered as one of the most dominant mycotoxins and maize cultivates in climates that show an extensive presence of the fungi, giving rise to permanent high aflatoxin contamination levels. We first characterize the fluorescence of pure aflatoxin B1. Subsequently, we study the OPIF and TPIF spectra of healthy and contaminated maize kernels, containing an aflatoxin B1 contamination lower than 1 ppb and higher than 70 ppb, respectively. The emission wavelengths and

intensities of the obtained spectra are investigated and a comparison between the performance of OPIF and TPIF is given. Afterwards, we examine the development of an optical detection criterion and study the localized contamination on the samples surfaces. Finally, we discuss the extensibility of our research methodology to other fluorescent mycotoxins.

2. Methodology and measurement set-up

We pursue a fluorescence measurement set-up suitable for both OPIF and TPIF fluorescence measurements. However, to obtain reliable measurement data, four challenges need to be tackled. (1) The selection of an optimal excitation wavelength is of major importance, to maximize the mycotoxin fluorescence and to minimize the influence of the intrinsic fluorescence signal. (2) The excitation spot size and excitation laser power should be optimized to enable the measurement of the weak mycotoxin fluorescence without damaging the food samples. (3) The natural variation within food products should be monitored, to assure we are measuring the influence of the toxin instead of the optical contrast between different product batches. (4) A careful selection of the products and the illumination positions on their surfaces is indispensable to deal with the localized presence of the mycotoxins. Due to the inhomogeneous presence of the toxin, measurements on individual products are much harder than optical measurements on homogeneous solutions and powders.

Keeping these challenges in mind, we first present our fluorescence measurement configuration, after which we explain the selection of the optimal excitation wavelengths.

2.1. OPIF and TPIF measurement set-up

To measure the OPIF and TPIF spectra of the localized contaminants, we require the generation of both UV and NIR illumination wavelengths, in combination with an accurate detection of the fluorescence signal while scanning the sample surface.

Generally, our measurement set-up can be divided into different building blocks, comprising an illumination laser system, the sample objective and the detecting optical spectrum analyser (**Figure 2**). A frequency-doubled Nd:YAG pump laser (Spectra-Physics Millennia Prime 10sJSPG) pumps a tunable titanium-sapphire laser (Spectra-Physics Tsunami laser). The wavelength of the titanium-sapphire laser can be tuned from 710 to 835 nm by the use of an internal slit, which selects the preferred wavelength after the dispersion of the generated laser light by internal prisms. The maximum output power ranges between 1.20 and 1.50 W, depending on the selected wavelength. The laser light of the titanium-sapphire laser can follow one out of two optical paths, depending on whether OPIF or TPIF measurements are performed (**Figure 2(a)**). For TPIF, the selected laser light is immediately directed towards the sample. In the case of OPIF, the fundamental laser light of the titanium-sapphire laser is directed towards a harmonic generating unit, comprising a second- and third-harmonic-generating crystal to generate the UV excitation wavelengths (**Figure 2(b)**). The second-harmonic-generating crystal is able to generate wavelengths between 355 and 417 nm, with a maximal output power between 200 and 450 mW. The third-harmonic-generating crystal enables us to use wavelengths between 240 and 275 nm, with a maximal output power between 60 and 200 mW. After the generation

of the UV light, by either the second- or third-harmonic-generating crystal, the laser light is directed towards the sample. During both OPIF and TPIF measurements, the sample is illuminated with a circular beam, with a spot diameter of 951 and 231 μm, respectively. To maximize the TPIF irradiance, the spot size of the illumination laser beam was minimized by the use of an additional focusing lens positioned in front of the sample (**Figure 2(d)**).
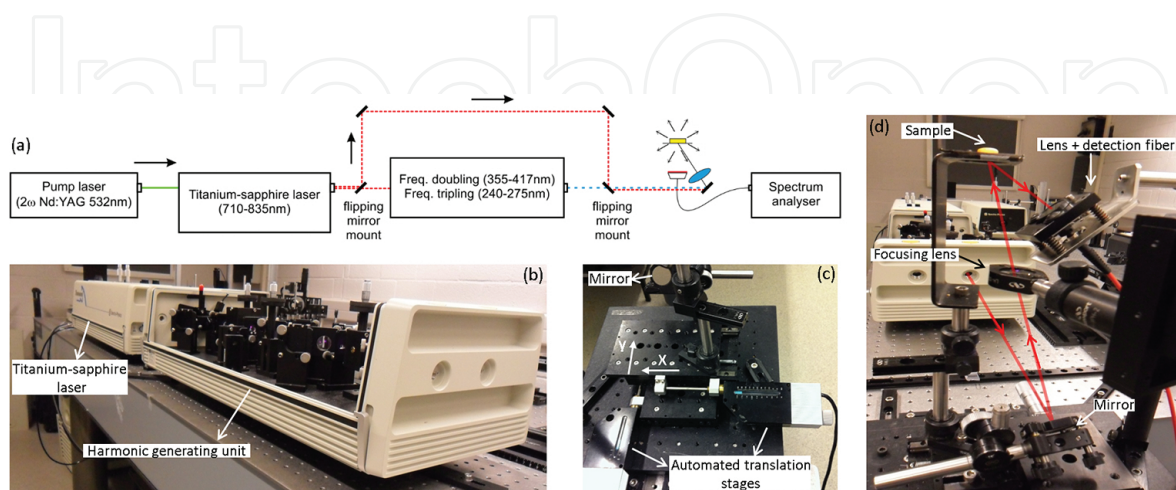

Figure 2. Measurement set-up that allows the investigation of both OPIF and TPIF: (a) schematic representation of the set-up; (b) tunable titanium-sapphire laser (710–835 nm) and harmonic generating unit with the frequency doubling (355–417 nm) and tripling crystals (240–275 nm); (c) automated translation stages on which the sample is mounted, enabling an accurate scanning in the X and Y direction; (d) optical path for the excitation of the sample, after which the fluorescence spectrum is captured by the detecting fibre. The focusing lens minimizes the spot size during the TPIF measurements.

The sample is positioned on a sample holder, containing a circular aperture with a diameter of 7 mm, enabling to position the kernels directly on this aperture. The sample holder is mounted on two automated translation stages (Newport 850G linear actuators) to accurately scan the product in both the X and Y direction (**Figure 2(c)**). For each X and Y position, the incident laser beam illuminates different parts of the product, allowing to study the localized contamination of the sample. Both automated translation stages have a travel range of 5 cm, scanning a maximum surface area of 25 cm^2. The translation stages are driven by a motion controller (Newport ESP300), enabling a high movement speed while assuring a high movement accuracy of 1 μm. During the scanning measurements, we use movement steps between 0.5 and 1.0 mm, as a trade-off between the measurement resolution and the illumination time of the sample. In order to avoid damage to the samples, the illumination time for each scanning measurement was restricted to 3 min, limiting the scanning resolution of the surface measurements.

After the excitation of the sample, the fluorescent signals are captured by a collimating lens, coupled into a broadband optical fibre (UVIR600 fibre of Avantes, transmitting light between 250 and 2500 nm) and guided towards the spectrum analyser (**Figure 2(d)**). We use a collimating lens in combination with a large fibre core diameter (600 μm) to obtain a total acceptance angle of 4.1°, allowing to capture the weak fluorescence signals of a surface area of 39 mm^2 (corresponding to the area within the circular aperture of the sample holder). In front of the

detecting fibre, we additionally mounted an interference-based filter to eliminate the excitation light. During the OPIF measurements, we implement a long-wave pass filter transmitting from 405 nm onwards (Semrock 405 nm EdgeBasic filter BLP01-405R-25), while during the TPIF measurements, a short-wave pass filter with a cut-on wavelength of 650 ± 5 nm is used (Newport 10SWF-650-B). Without the use of an optical filter, the excitation signals would saturate the measured fluorescence spectrum, leading to incorrect measurement data. Furthermore, we make use of the AvaSpec2048 spectrum analyser, which is able to measure the spectrum between 300 and 1100 nm with a resolution of 8 nm. This instrument has a wide entrance slit of 200 μm that allows capturing the weak fluorescence signals.

To obtain the absolute fluorescence spectrum of a sample, the measured spectra are corrected by a transfer function, taking the wavelength-dependent transmittance of the optical fibre and the sensitivity of the detector inside the spectrum analyser into account. This transfer function was obtained after the measurement of a calibrated light source with an a priori known absolute spectrum. We first connected the calibration light source to the spectrum analyser by using the UVIR600 fibre. Following, we measured the spectrum of the calibration light source and compared the measured photon counts for each wavelength with the specified output power of the manufacturer, in μW/cm². Using this measurement data, the Avasoft 8 software is able to calculate the absolute fluorescence spectrum (in μW/cm²/nm) of a sample (I_{sample}), by using the following equation [21]:

$$I_{sample}(\lambda) = \text{Caldata}(\lambda) \frac{\text{sample}(\lambda) - \text{dark}(\lambda)}{\text{refcal}(\lambda) - \text{darkcal}(\lambda)} \frac{\text{Int}_{cal}}{\text{Int}_{sample}}$$ (1)

With Caldata(λ) the intensity of the calibrated light source in μW/cm², obtained from the manufacturer; sample(λ) the measured spectrum of the sample, in A/D counts; dark(λ) the dark signal during the sample measurements, in A/D counts; refcal(λ) the measured spectrum of the calibrated light source, in A/D counts; darkcal(λ) the dark signal during the measurements with the calibrated light source, in A/D counts; Int_{cal} the integration time during the measurements of the calibrated light source; and Int_{sample} the integration time during the measurements of the sample.

During the fluorescence characterization measurements, a study of the fluorescence intensity as function of the excitation power is essential. Therefore, the excitation laser power is tuned by mounting attenuation filters behind the laser output, in front of the tilted mirror (mirror indicated in **Figure 2(d)**; the attenuation filters are not presented in this picture).

2.2. Selection of the excitation wavelengths

To maximize the mycotoxin fluorescence intensity, we select an excitation wavelength that is strongly absorbed by the mycotoxins, since an increasing amount of absorbed photons gives rise to an increasing amount of excited electrons and thus also to an enlarged number of fluorescent photons. Furthermore, by using an excitation wavelength with a strong mycotoxin

absorbance, the influence of the mycotoxin fluorescence emission onto the natural fluorescence spectrum of the food products can be maximized. When considering the absorption spectrum of aflatoxin B1, ochratoxin A and zearalenone, the strongest absorbances are observed within the 200–400-nm spectral region (**Figure 3(a)**) [9]. Specifically, aflatoxin B1 shows the strongest absorbance in the range between 200 and 275 nm and around 365 nm. Ochratoxin A has a strong absorbance between 200 and 250 nm and around 335 nm, while zearalenone shows a strong absorbance in the 200–350 nm spectral range.
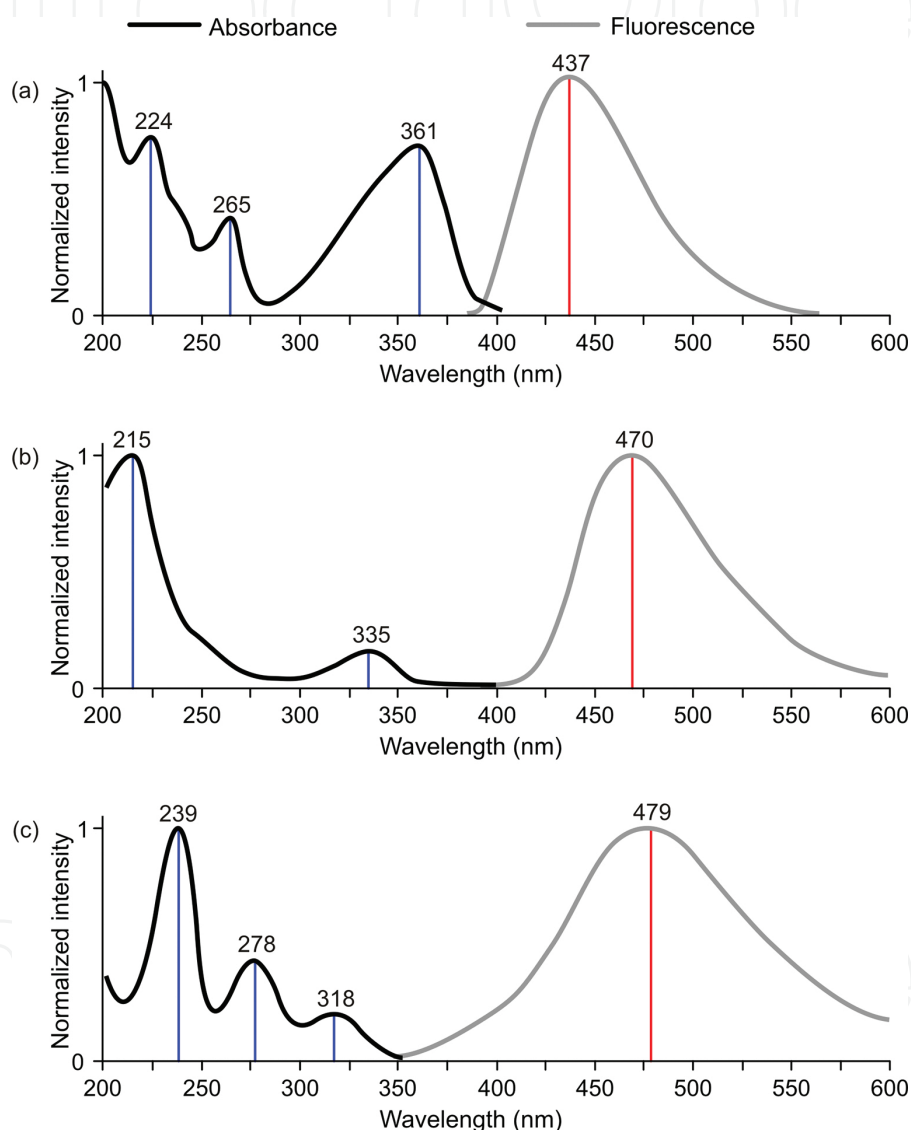
Figure 3. Absorbance and fluorescence spectrum of fluorescent mycotoxins: (a) aflatoxin B1, (b) ochratoxin A, (c) zearalenone.

In addition to the absorbance of the mycotoxins, the intrinsic fluorescence of the food products needs to be taken into account. Food products often contain several proteins that show fluorescence emission after excitation with certain wavelengths [22]. For example, maize contains the fluorescent proteins tryptophan (Trp), tyrosine (Tyr) and phenylalanine (Phe),

which all show a strong absorbance in the 200–300 nm wavelength range (**Figure 4**). If we would excite maize kernels with a wavelength between 240 and 275 nm, the fluorescence of these proteins would disturb our measurements. The proteins show no fluorescence after excitation with 355–417 nm light, since they only show a weak absorbance from 300 nm onwards.
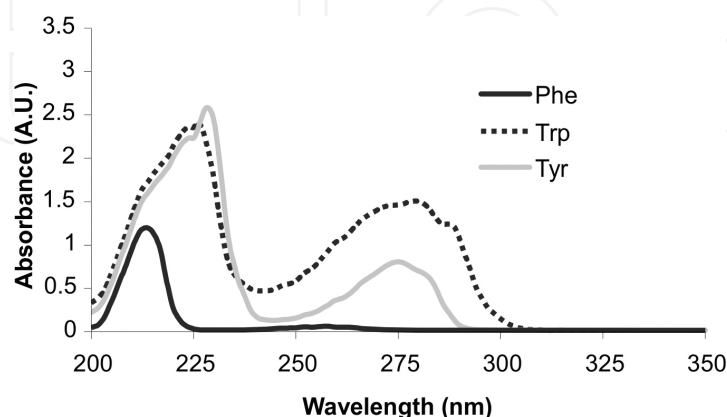

Figure 4. Absorbance spectrum of different fluorescent proteins in maize: phenylalenine (Phe), tryptophan (Trp) and tyrosine (Tyr) [22].
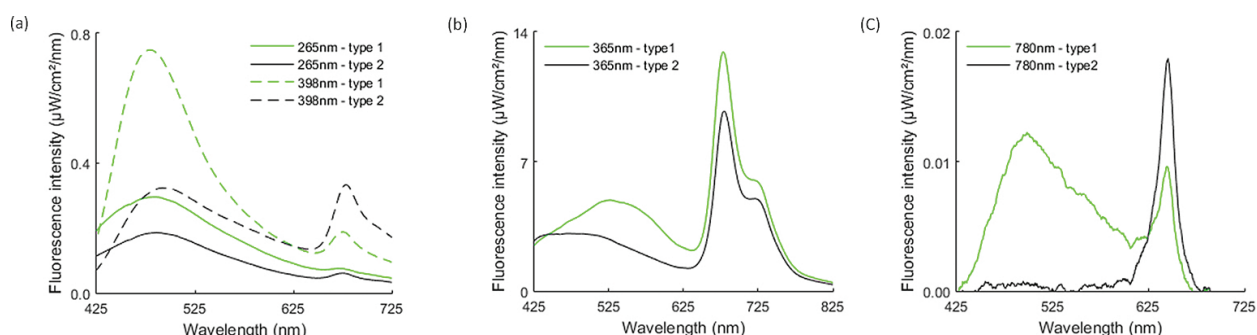

Figure 5. Intrinsic fluorescence of healthy food products: (a) OPIF of coffee beans after excitation with 265 and 398 nm, (b) OPIF of pistachio nuts after excitation with 365 nm, (c) TPIF of pistachio shells after excitation with 780 nm.

Furthermore, also the natural variation within food products should be examined during the fluorescence measurements. Due to the large internal variation in density, texture and substituents concentration, various batches of a product type can show different fluorescence spectra or intensities. As an illustration, we present the intrinsic fluorescence of healthy coffee beans and pistachio nuts, showing significant differences within the fluorescence spectra of different batches (**Figure 5**). When illuminating two batches of coffee beans with 265 and 398 nm laser light, different ratios of the local fluorescence maxima at 480 and 680 nm can be observed for each batch (**Figure 5(a)**). Two varieties of pistachio nuts, after illumination with 365 nm, show a different fluorescence spectrum between 425 and 625 nm, with a maximal difference at 530 nm (**Figure 5(b)**). Both types of pistachio nuts do show chlorophyll fluorescence, present between 625 and 825 nm. Considering the outer pistachio shells, after illumi-

nation with 780 nm, a clear contrast between the fluorescence of both pistachio types can be identified between 425 and 625 nm (**Figure 5(c)**). The fluorescence spectrum of the first type shows a clear two-photon-induced fluorescence signal between 425 and 625 nm and a chlorophyll fluorescence maximum at 645 nm, while the second type only shows chlorophyll fluorescence. As a result, to account for the natural variation, different independent sets of products should always be compared.

Finally, when selecting the excitation wavelengths, we keep in mind the commercial available laserlines. We prefer using commercially available wavelengths to enable the integration of our developed optical detection criterion into industrial scanning-based sorting devices.

When considering our case study, the sensing of the aflatoxin contamination in maize kernels, we use an excitation wavelength of 365 nm during the OPIF measurements, since at this wavelength, the absorbance of the aflatoxin B1 is maximized, while the absorbance of the proteins is minimized. Consequently, to study the TPIF spectrum, excitation wavelengths close to 730 nm are required. In addition, when studying the maize kernels, we also investigate the fluorescence spectrum after excitation with 750 and 780 nm, to study the influence of the matrix constituents onto the fluorescence spectrum.

3. Case-study: localized detection of the aflatoxin contamination

As a case study, we focus on the detection of the localized aflatoxin contamination in individual maize kernels. Specifically, within this section, we present an in-depth explanation of our research methodology, giving rise to the development of an accurate optical sensing criterion. We first characterize the OPIF and TPIF spectra of pure aflatoxin, after which we investigate the fluorescence properties of the healthy and contaminated maize kernels.

3.1. Characterization of the aflatoxin fluorescence spectrum

Aflatoxin is one of the most dominant and toxic mycotoxins. It is produced by the fungi *Asperigullus flavus* and *Asperigullus parasiticus*. To perform a basic characterization of the fluorescence properties of aflatoxin, we measured the OPIF and TPIF spectrum of pure aflatoxin B1 powder (98% or better purity, produced by the *A. flavus* fungi) that we purchased from Sigma-Aldrich. It is a white to yellow crystalline powder that we measured in its solid state.

We present the mean OPIF and TPIF spectra of pure aflatoxin B1 powder (**Figure 6**). The OPIF spectrum is obtained after excitation with 365 nm, with an excitation power density of 42 mW/mm^2, while the TPIF spectrum is measured after excitation with 730 nm, with an excitation power density of 14.3 W/mm^2. Both fluorescence spectra show their maximal fluorescence intensity at 428 nm, which corresponds with the expected aflatoxin B1 fluorescence maximum (**Figure 3(a)**). The OPIF spectrum shows higher fluorescence intensities than the TPIF spectrum. The maximal OPIF intensity (at 428 nm) is equal to $1.68 \pm 0.93 \ \mu W/cm^2$, while we observe a maximal TPIF intensity of $0.20 \pm 0.09 \ \mu W/cm^2$. The measured TPIF intensity is hence 10 times

weaker than the OPIF intensity. The shape of the TPIF spectrum shows a narrower peak than the OPIF spectrum due to the more selective excitation during two-photon absorption than during one-photon absorption. Furthermore, in the TPIF spectrum at 365 nm, we observe a second-harmonic generation signal. This peak is created by the recombination of two illumination photons to a new photon with the double energy. Around 400 nm, the OPIF spectrum shows a steeper slope than the TPIF spectrum, because of the presence of a long-wave pass filter suppressing light below 405 nm during the OPIF measurements.
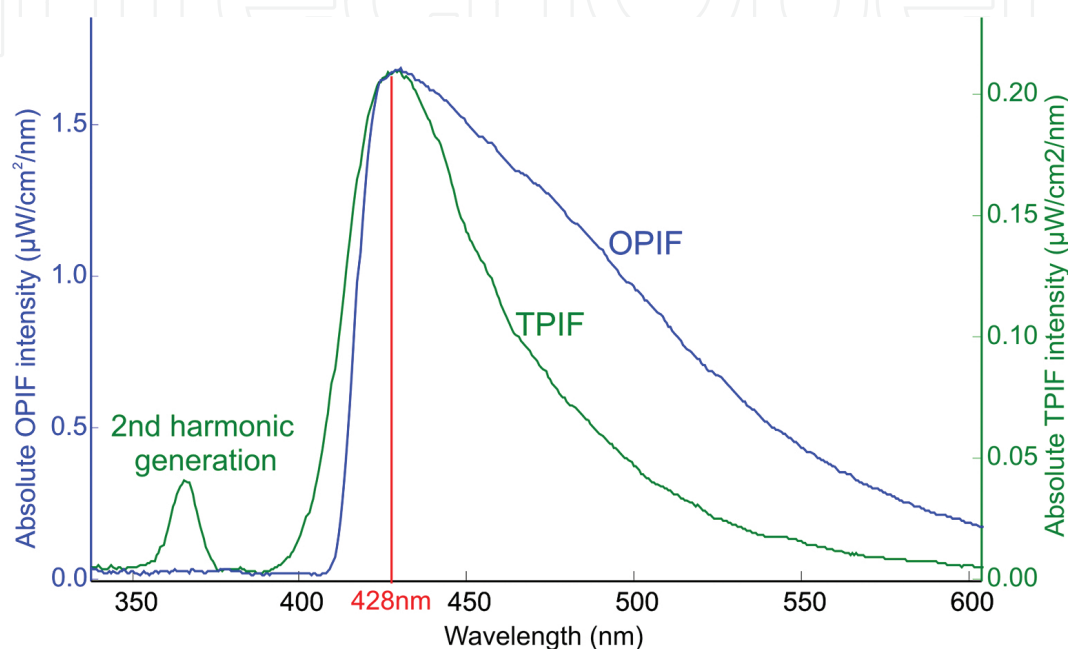

Figure 6. OPIF and TPIF spectra of the pure aflatoxin B1 powder, after excitation with 365 and 730 nm, respectively.

To characterize the aflatoxin B1 fluorescence spectrum, we studied the integrated fluorescence intensity as function of the excitation power, while maintaining a constant spot diameter of 951 μm during the OPIF measurements and 231 μm during the TPIF measurements (**Figure 7**). For each excitation power, we integrated the measured mean fluorescence spectrum between 400 and 600 nm to obtain the depicted integrated fluorescence intensity. Studying the integrated OPIF intensity as function of the excitation laser power, we observe a linear relationship, representing the linear one-photon absorption. However, at higher excitation powers, starting from 35 mW onwards, the integrated OPIF intensity deviates from the linear relationship and starts saturating. In the saturated region, the maximum fluorescence intensity is reached since then all electrons are excited to the higher energy state. The TPIF intensity shows a quadratic dependence on the excitation laser power, confirming the occurrence of non-linear two-photon absorption. Moreover, we can observe that TPIF requires much higher excitation powers, starting from 100 mW onwards. The variation of the measured data is less than 10 and 12% during the OPIF and TPIF measurements, respectively. Both the linear and exponential fits show an adjusted r-square value of 0.98 and 0.97, respectively, ensuring that the fitted function is a good representation of the measured data.

TPIF requires a higher excitation power density than OPIF [23]. The minimal excitation power density for OPIF is 5 mW/mm^2, while TPIF requires a minimal power density of 2 W/mm^2. As a result, the measurement constraints are more severe for TPIF than for OPIF. A high excitation power, a small spot size and a sensitive detector are indispensable to measure TPIF signals. However, considering the implementation in practical applications, TPIF uses NIR excitation wavelengths which are more widely commercially available than the required UV excitation wavelengths for OPIF.
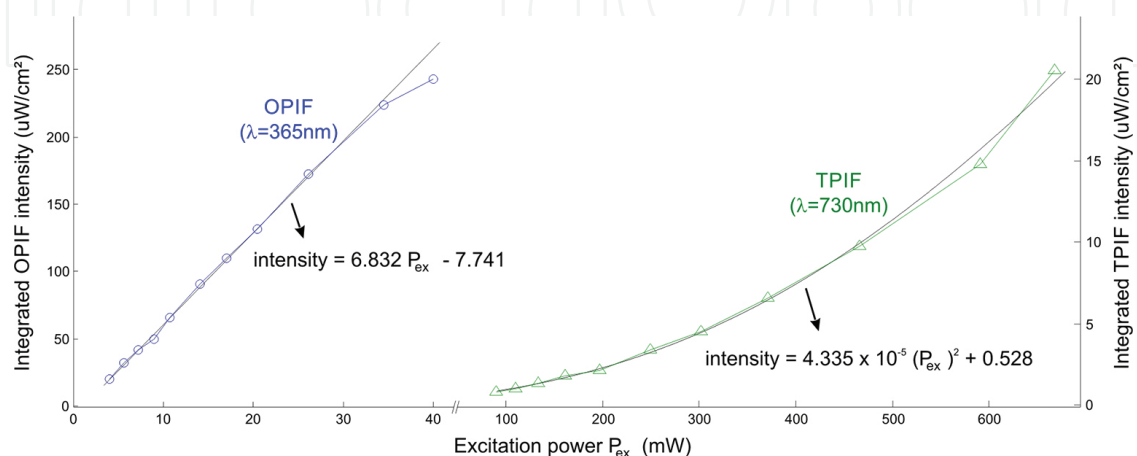

Figure 7. Intensity of the integrated OPIF spectrum increases linearly with the excitation power, while the intensity of the integrated TPIF spectrum shows a quadratic dependence on the excitation power.
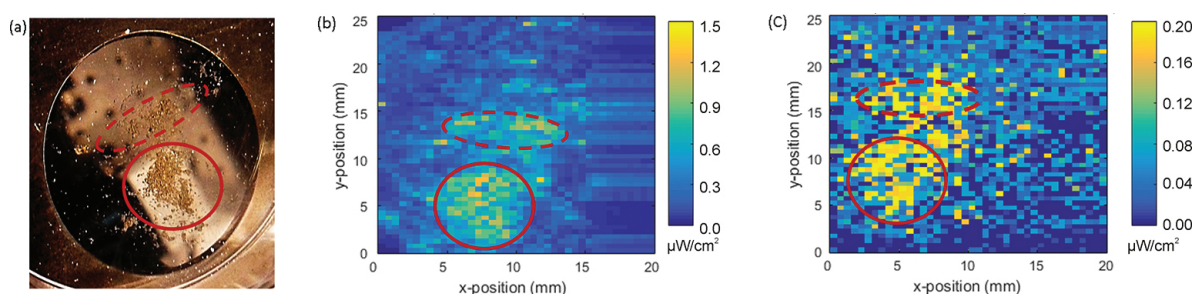

Figure 8. Scanning of the aflatoxin B1 powder, visualizing the location of the emitted fluorescence signals: (a) aflatoxin B1 power, (b) OPIF surface plot and (c) TPIF surface plot, indicating the localized fluorescence intensity at 428 nm.

To validate the automated screening of the samples, a scanning of the pure aflatoxin B1 powder is performed (**Figure 8**). Particularly, we consider a Petri dish on which the aflatoxin B1 powder is disposed in two separate areas, of which we screen an area of 20.0 mm by 25.0 mm, with a resolution of 0.5 mm. By adjusting the X and Y position of the automated translation stages, while measuring the fluorescence signal for every position, the aflatoxin powder can be identified (indicated by the solid and dotted circles in **Figure 8**). During both the OPIF and TPIF measurements, the aflatoxin B1 fluorescence is detected. The encircled regions in the surface plots indicate the areas from which a minimum fluorescence intensity of 0.8 and 0.1 μW/cm^2 at 428 nm is detected during the OPIF and TPIF measurements, respectively. The

aflatoxin powder consists of granules positioned at two areas on the Petri dish (**Figure 8(a)**). If a small aflatoxin granule is illuminated, we detect a fluorescence signal. However, we obtain a smoother surface plot for OPIF than for TPIF, due to the larger spot diameter of the illumination beam (951 μm) during the OPIF measurements. During the OPIF measurements, most illumination positions around the powder excite one or multiple aflatoxin granules, since the surface area in-between the granules is smaller than the spot diameter. When using a smaller spot diameter, like during the TPIF measurements (231 μm), no fluorescence signal can be captured when the illuminating beam is positioned in-between the aflatoxin granules. Consequently, a more fragmented surface plot is obtained (**Figure 8(c)**).

Generally, our fluorescence measurements of the pure aflatoxin B1 powder correspond with the theoretical characteristics, validating a correct measurement of the fluorescence signals. In addition, the powder could be successfully visualized, indicating a good operation of the automated scanning of the samples.

3.2. Sensing of the localized aflatoxin contamination in maize kernels

We investigate the sensing of aflatoxin-contaminated maize kernels by using fluorescence spectroscopy. We first give an overview of the investigated samples. Following, we study the OPIF and TPIF spectra of healthy and contaminated maize kernels, including the investigation of the intrinsic fluorescence spectra and its dependency on the excitation wavelength. Based on this study, we develop a detection criterion enabling to sense the contaminated kernels. Finally, the detection of the localized contamination areas onto the kernel's surfaces are studied and visualized with surface plots.

3.2.1. Overview of the investigated samples

We consider two different independent maize batches, each with a healthy and contaminated subsample. One healthy and one contaminated maize batch were harvested in 2012 and provided by an Italian company. The second set of healthy and contaminated maize samples was collected from Croatian farmers, after the harvest in 2013. From each maize batch, a subsample of 25 g was drawn for the analytical determination of the aflatoxin contamination level. Each sample was chemically analysed using the ToxiQuant mycotoxin testing system of ToxiMet [24]. Considering the Italian maize kernels, the contaminated sample shows 72.1 ppb aflatoxin B1 and the healthy one 0.0 ppb. The maize samples from Croatia show approximately the same aflatoxin B1 contamination level, being 78.9 ppb for the contaminated sample and 0.8 ppb for the healthy sample. After our measurements were performed, the contamination level of the maize samples was confirmed by the CODA-CERVA, the Belgian Reference Laboratory for Mycotoxins. Comparing the contamination levels with the international regulations, both the Italian and Croatian contaminated batches can be considered as highly contaminated. The European Commission states the maximum allowed total aflatoxin concentration in maize to be 10 ppb, while the USA food safety regulations included a limit of 20 ppb of total aflatoxins in all food products [12].

During our fluorescence measurements, we investigated the fluorescence spectra of 45 healthy and contaminated Croatian maize kernels to obtain a statistic relevant distribution of our measurement data. To observe the influence of the sample type and the harvest environments on the fluorescence spectra, we also measure the fluorescence spectra of 15 healthy and contaminated Italian maize kernels. The Italian company provided only small maize batches, which limits the number of studied maize kernels, but is sufficient to monitor the environmental influences on the spectra. Because aflatoxin is sensitive to light, the samples are permanently stored in a dark enclosure to reduce the environmental influences onto the measurements. In-between the measurements, the samples are stored in a fridge to avoid cross-contamination.

3.2.2. OPIF and TPIF spectra of the maize kernels

To investigate the optical detection of aflatoxin B1, we study the OPIF and TPIF spectra of healthy and contaminated maize kernels of both the Croatian and Italian maize batches. We measured the OPIF spectrum after excitation with 365 nm, with an excitation power density of 317 mW/mm^2 (**Figure 9(a)**). The TPIF spectra are measured after excitation with 730, 750
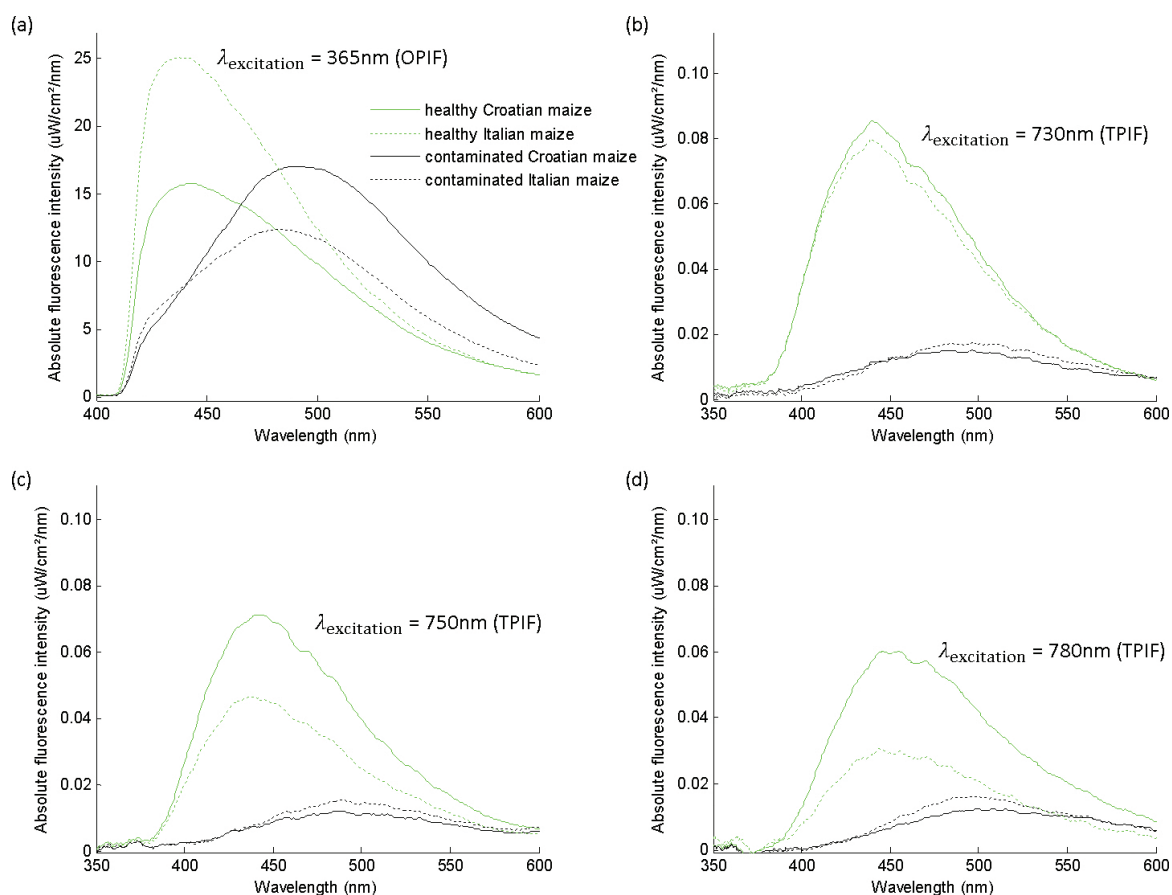

Figure 9. Fluorescence spectra of the healthy and contaminated maize kernels of the Croatian and Italian maize batches: (a) OPIF spectrum after excitation with 365 nm; TPIF spectrum after excitation with (b) 730 nm, (c) 750 nm and (d) 780 nm.

and 780 nm, with an excitation power density of 26.2, 29.1 and 36.0 W/mm^2, respectively
(**Figure 9(b)**, **(c)** and **(d)**). During the TPIF measurements, we investigate the fluorescence
spectrum after excitation with multiple wavelengths to monitor the influence of the illumina‐
tion wavelength onto the fluorescence emission of the maize kernels. To maximize the signal
to noise ratio, we illuminate the maize kernels with the maximal output power of the titanium‐
sapphire laser and harmonic generating unit. However, we limited the measurement time to
20 and 200 ms for the OPIF and TPIF measurements, respectively, to avoid damage to the
sample surface. For every maize batch, the mean fluorescence spectrum is depicted. Both the
healthy and the contaminated samples show a fluorescence signal due to the intrinsic
fluorescence of the maize kernels (**Figure 9**). On the basis of these measurements, a compre‐
hensive evaluation can be made by comparing the fluorescence spectra of the Italian and
Croatian maize batches, by evaluating the performance of OPIF and TPIF and by defining the
spectral differences between the healthy and contaminated samples.

Excitation wavelength	Maximum fluorescence intensity			
	Croatian maize (μW/cm^2/nm)		Italian maize (μW/cm^2/nm)	
	Healthy	Contaminated	Healthy	Contaminated
365 nm	15 ± 8	17 ± 10	25 ± 17	13 ± 9
730 nm	0.09 ± 0.05	0.02 ± 0.01	0.08 ± 0.05	0.02 ± 0.01
750 nm	0.07 ± 0.03	0.02 ± 0.01	0.05 ± 0.02	0.02 ± 0.01
780 nm	0.06 ± 0.04	0.02 ± 0.01	0.03 ± 0.01	0.02 ± 0.01

Table 1. Measured maximum fluorescence intensity and its variation for the different excitation wavelengths.

Considering the different maize batches, the fluorescence spectra of the Croatian and Italian
maize correspond well within the variances of the measurements (**Table 1**). For all excitation
wavelengths, both maize types emit corresponding fluorescence signals, showing a similar
spectral shape in the same wavelength regions. The present intensity variances are caused by
the differences within the molecular structure of the maize kernels. Because maize is a natural
product, the maize kernels show a large internal variation in surface shape, density and natural
composition. In correspondence with the measurements on the pure aflatoxin B1 powder, the
fluorescence intensity induced by one-photon excitation is much stronger than the intensity
induced by two-photon excitation. Specifically, the OPIF signal is approximately 500 times
stronger than the TPIF signal.

Comparing the fluorescence spectra of the healthy and contaminated maize kernels, we
observe significant differences in intensity and emission wavelength. We do not observe the
aflatoxin fluorescence directly, but we measure its influence on the intrinsic fluorescence of the
maize. In the contaminated samples, the aflatoxin is bonded to the different natural constitu‐
ents of the healthy maize, changing the molecular structure of the constituents and therefore
influencing the intensity and wavelength of the emitted fluorescence signals. During both the
OPIF and TPIF measurements, we observe higher fluorescence intensities for the healthy maize
kernels than for the contaminated ones (**Table 1**). The intensity contrast is the largest for the

TPIF spectra, since the different bonds inside the maize are more selectively excited during the TPIF process than during the OPIF one. The largest intensity differences between the healthy and contaminated samples are observed after excitation with 730 nm, where the mean fluorescence intensity of the healthy maize is four times stronger than the mean fluorescence intensity of the contaminated maize. In contrast, the minimum intensity differences are observed after excitation with 365 nm. The observed large intensity variations within the healthy and contaminated samples are caused by a combination of the curved surface of the maize kernels and the non-homogeneous presence of the toxins inside the maize.

In addition to the fluorescence intensity differences, we observe a wavelength shift between the fluorescence maxima of the healthy and contaminated maize samples (**Table 2**). Generally, the OPIF and TPIF spectra show a wavelength shift of approximately 50 nm. To compare the obtained wavelength shift for the different excitation wavelengths, we calculate the class difference for both the Croatian and Italian maize. The class difference (D) is a measure for the difference between the average values (μ) of two product types, taking the standard deviation (σ) and the amount of measured samples (N) into account [25]:

$$D = \frac{\left|\mu_{\text{contaminated}} - \mu_{\text{healthy}}\right|}{\sqrt{\dfrac{\sigma^2_{\text{contaminated}}}{N_{\text{contaminated}}} + \dfrac{\sigma^2_{\text{healthy}}}{N_{\text{healthy}}}}} \qquad (2)$$

Excitation wavelength	Dominant emission wavelength Croatian maize (nm)		Class difference Croatian maize	Dominant emission wavelength Italian maize (nm)		Class difference Italian maize
	Healthy	Contaminated		Healthy	Contaminated	
365 nm	443 ± 5	497 ± 15	9.7	442 ± 5	486 ± 6	10.8
730 nm	441 ± 3	496 ± 20	6.1	441 ± 3	496 ± 16	4.1
750 nm	444 ± 7	497 ± 24	3.8	440 ± 5	490 ± 17	2.7
780 nm	450 ± 10	503 ± 19	5.2	450 ± 7	498 ± 10	4.8

Table 2. Emission wavelength at maximum fluorescence intensity and its variation for the different excitation wavelengths.

The OPIF measurements show the largest class differences, indicating the largest optical contrast between the healthy and contaminated maize kernels. The variation of the class differences between the OPIF and TPIF measurements are mainly caused by their different variances. The TPIF spectra show a larger variance than the OPIF spectra, which decreases their class difference. TPIF signals show a weaker intensity, resulting in a stronger relative noise signal and therefore a lower signal to noise ratio.

To validate the influence of the aflatoxin onto the intrinsic fluorescence spectrum of the maize, we tune the excitation wavelength towards the wavelengths for which aflatoxin B1 shows a

weaker absorbance. We measured the fluorescence spectrum of healthy and contaminated maize kernels after excitation with 405 and 810 nm laser light, during the OPIF and TPIF measurements, respectively (**Figure 10**). Both the OPIF and TPIF measurements show a small difference between the fluorescence spectrum of the healthy and contaminated samples. We measure a wavelength shift of 8 ± 6 nm and 26 ± 12 nm, after excitation with 405 and 810 nm, respectively. Moreover, we observe only small differences between the fluorescence intensities. Because aflatoxin B1 shows a weak absorbance at 405 nm (**Figure 3(a)**), it only minimally influences the intrinsic fluorescence spectrum of the maize kernels.
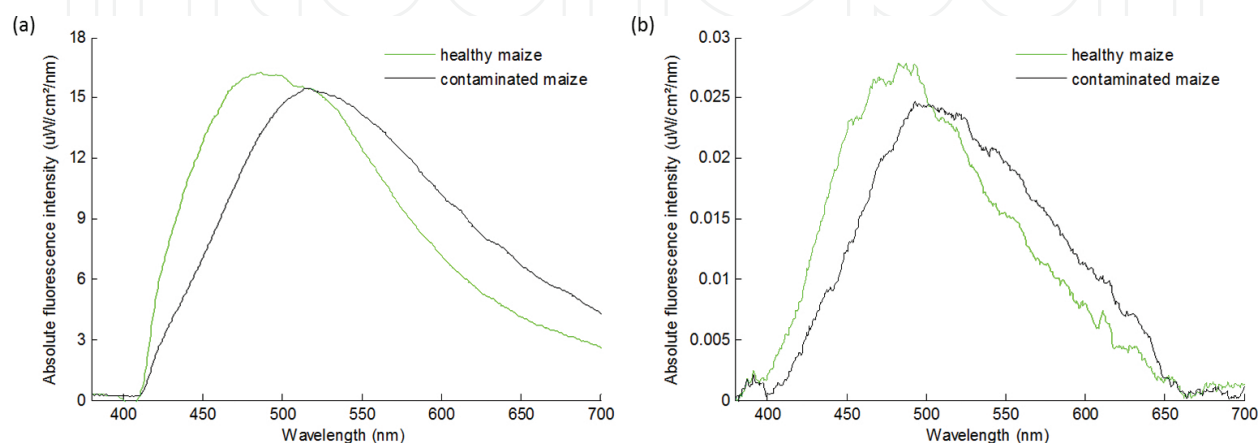
Figure 10. Fluorescence spectra of the healthy and contaminated maize kernels: (a) OPIF spectrum after excitation with 405 nm and (b) TPIF spectrum after excitation with 810 nm.

Summarized, both OPIF and TPIF show a spectroscopic contrast between the healthy and contaminated maize kernels. In the next step, we use the above quantitative evaluation to define and test our optical detection criterion.

3.2.3. Development of an optical detection criterion

To obtain an accurate optical detection criterion, taking the shape, intensity and maximum emission wavelength of the fluorescence spectra into account, we examine the integral of the fluorescence spectra in various wavelength intervals. Keeping in mind the wavelength ranges of the fluorescence spectra and the maximum fluorescence intensities, both depicted in **Figure 9** and presented in **Tables 1** and **2**, we obtain an optimal contrast between the healthy and contaminated samples by considering the ratio of the integrated fluorescence intensity from 475 to 550 nm and the integrated fluorescence intensity from 400 to 475 nm. When visualizing the ratio of these integrals for each maize kernel, a clear distinction between the healthy and contaminated samples is visible (**Figure 11**). Particularly, the ratios show a minimum contrast of 0.24, 0.13, 0.19, 0.25 and a maximum contrast of 2.15, 1.93, 2.87, 3.39 for excitation with 365, 730, 750 and 780 nm, respectively. The largest difference between the mean ratio of the healthy and contaminated samples is observed after excitation with 780 nm. Considering the class differences of the integral ratio between the healthy and contaminated samples, we obtain a value of 116.2, 111.1, 48.8 and 54.9 for excitation with

365, 730, 750 and 780 nm, respectively. The largest class difference can thus be found after excitation with 365 nm. Regarding the TPIF measurements, the largest class difference is obtained after excitation with 780 nm. The TPIF measurements show generally a smaller class difference than the OPIF ones, due to their larger measurement variation. However, the contaminated samples can still be properly identified with TPIF, allowing using NIR excitation wavelengths, instead of the UV wavelengths for OPIF.
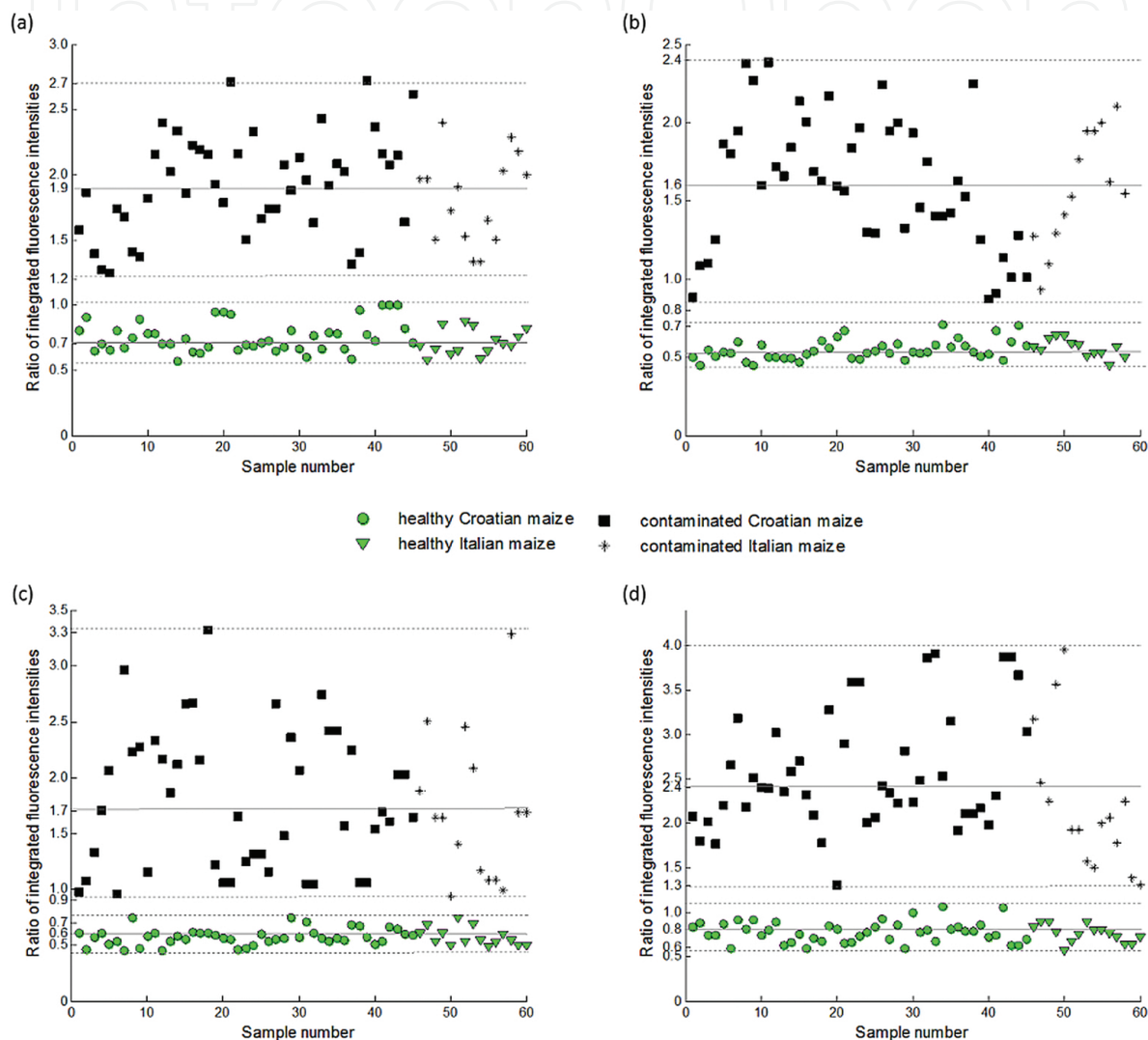
Figure 11. Contrast between the fluorescence spectra of the healthy and contaminated maize samples, visualized by the ratio of the integrated fluorescence spectrum from 475 nm until 550 nm to the integrated fluorescence spectrum from 400 nm until 475 nm, after excitation with (a) 365 nm, (b) 730 nm, (c) 750 nm and (d) 780 nm.

The ratios of the integrated fluorescence intensities of the contaminated samples generally show a larger variation than the ratios of the healthy samples, because of the localized presence of the aflatoxin and the variable aflatoxin concentration in the maize kernels. Depending on the illumination position on the maize kernel's surface, a different contamination level may be present, influencing the wavelength and intensity of the fluorescence spectrum. To visualize

the localized aflatoxin contamination on the maize kernel's surfaces, scanning measurements needed to be performed.

3.2.4. Monitoring of the localized presence of the aflatoxin

To monitor the localized presence of the aflatoxin, we scanned the maize kernels by using the automated translation stages. We investigated the localized aflatoxin contamination when illuminating the samples with 365 and 780 nm laser light, since these wavelengths showed the largest spectroscopic differences during the OPIF and TPIF measurements, respectively [26].
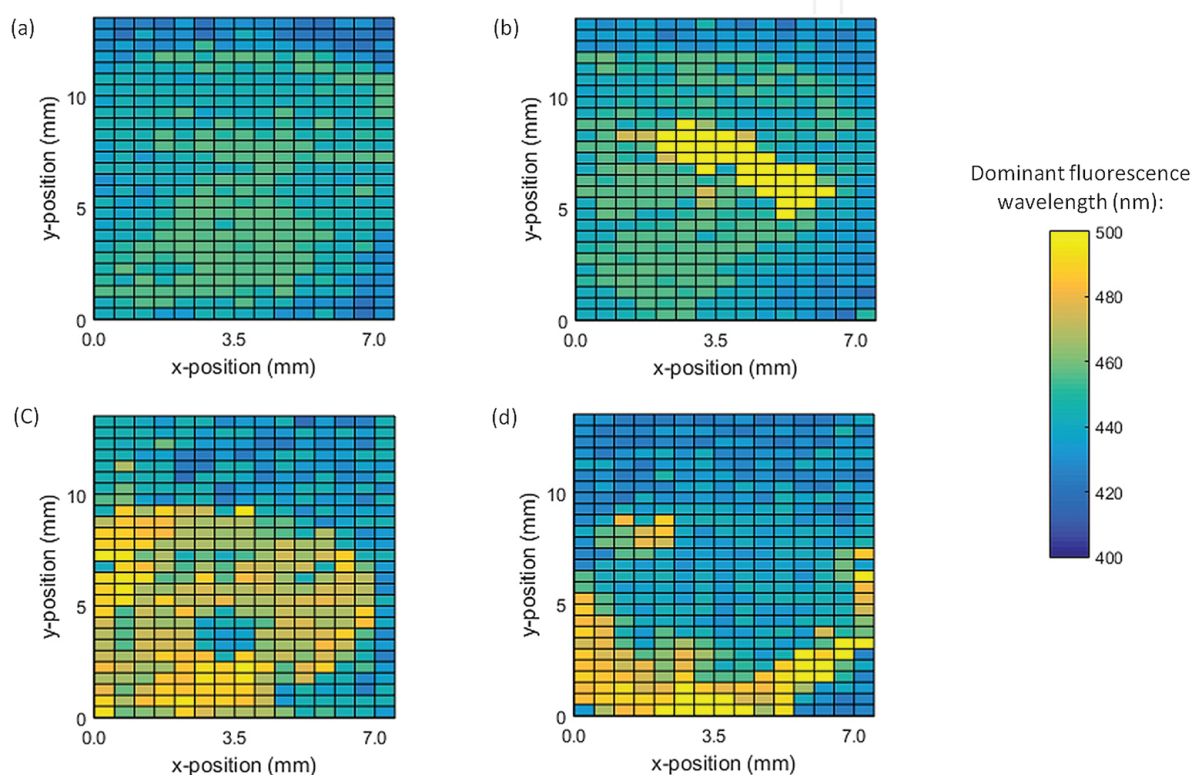
Figure 12. Visualization of the localized aflatoxin contamination, measured during OPIF, by mapping the dominant fluorescent emission wavelength along the kernel's surface: (a) healthy kernel, (b) kernel with a small localized contamination area, (c) kernel with homogeneous contamination and (d) kernel with a medium to large contamination at the edge.

During the OPIF measurements, we scanned the maize kernels with a resolution of 0.5 mm. For every sample, we recorded 405 spectra, each of which corresponding with a different illumination position of the laser beam. Considering the fluorescence wavelength showing the maximum fluorescence intensity, different regions in the kernels can be identified (**Figure 12**). In correspondence with the previous measurements, the fluorescence spectra of the healthy maize kernels show their maximum fluorescence intensity between 400 and 450 nm (**Figure 12(a)**). The contaminated areas show their maximum fluorescence intensity at wavelengths longer than 450 nm. By interpreting the surface plots, various areas containing different contamination levels can be observed on differ-

ent positions of the kernel's surface (**Figure 12(b)**, **(c)** and **(d)**). As an example, the contaminated kernels can show a small localized contaminated area, a homogeneous contamination along the maize kernel or a medium to large contamination at the edge of the kernel. When considering the ratio of the integrated fluorescence spectra, specifically the ratio of the integrated fluorescence intensity between 475 and 550 nm and the integrated fluorescence intensity between 400 and 475 nm, a similar observation can be made (**Figure 13**). In correspondence with **Figure 11**, the high-contaminated areas show the largest ratios. Furthermore, the gradient of the contamination level is clearly visible. When considering **Figure 13(b)**, two highly contaminated areas surrounded by a medium-contaminated area can be identified, while **Figure 13(d)** shows a highly contaminated area at the edge that flows into a healthy area in the centre of the kernel. Concluding, localized contaminated areas can be accurately identified and characterized by mapping the integral ratio on the screened kernel's surfaces.
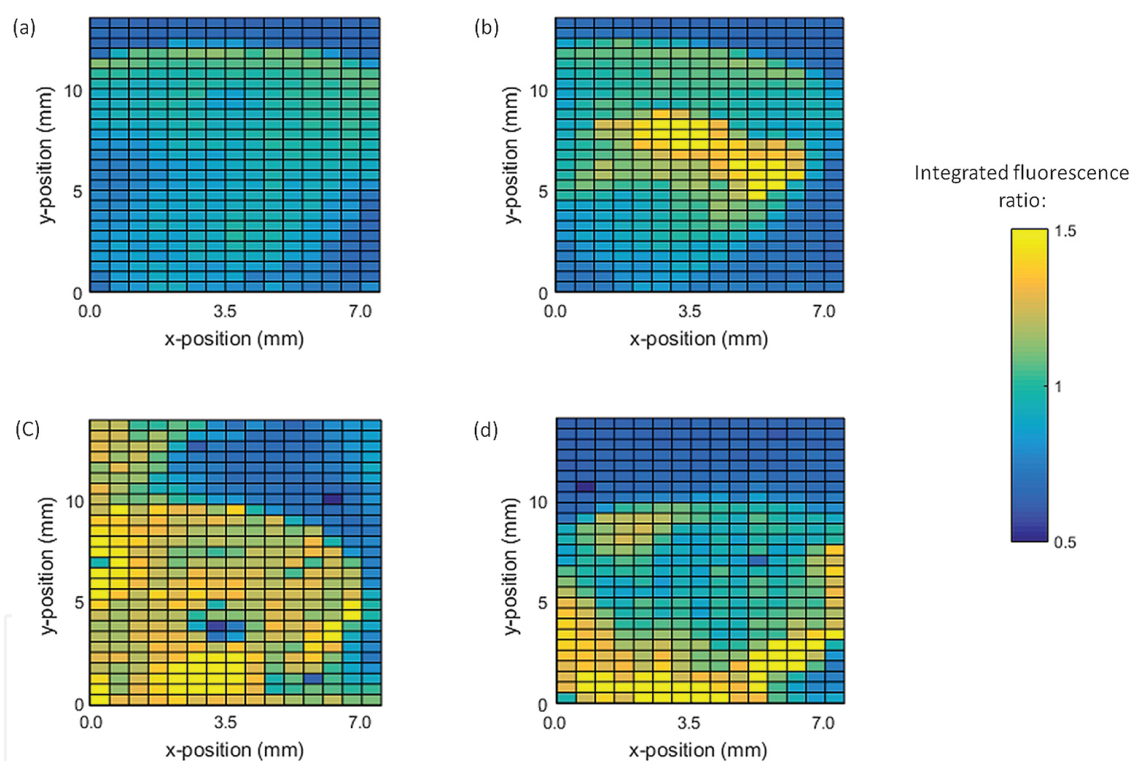

Figure 13. Visualization of the localized aflatoxin contamination during OPIF, by mapping fluorescence ratios (integrated fluorescence intensity between 475 and 550 nm divided by the integrated fluorescence intensity between 400 and 475 nm) along the kernel's surface: (a) healthy kernel, (b) kernel with small localized contamination area, (c) kernel with homogeneous contamination and (d) kernel with a medium to large contamination at the edge.

Considering the TPIF measurements, the maize kernels could only be partially scanned with a lower resolution of 1 mm (instead of the 0.5 mm resolution used during the OPIF scanning measurements). When accurately scanning a complete maize kernel's surface during the TPIF measurements, the kernel's surface would be damaged, due to the required long illumination time and high illumination power density. Specifically, the illumination time is significantly

longer during the TPIF measurements than during the OPIF measurements (approximately 10 times longer) due to the longer measurement time of the spectrum analyser required to capture the weak TPIF signals. Consequently, to avoid measuring the influence of damaging effects, the kernels are measured with a lower accuracy (**Figure 14**). Studying the corresponding surface plots, regions with a high and low contamination level can still be observed. Specifically, the regions with a dominant fluorescence wavelength longer than 450 nm can be considered as contaminated. Furthermore, the longer the fluorescence wavelength, the higher the contamination level on the kernel's surface. The maize kernel depicted in **Figure 14(a)** shows generally a lower contamination than the one depicted in **Figure 14(b)**.
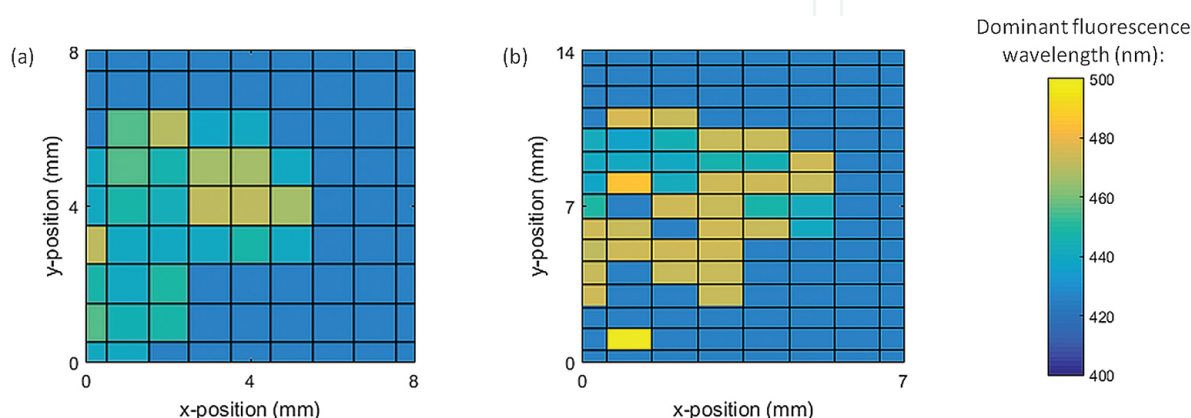

Figure 14. Visualization of the localized aflatoxin contamination during TPIF, by mapping the dominant fluorescent emission wavelength along the kernel's surface: (a) low-contaminated kernel and (b) high-contaminated kernel.

The scanning plots demonstrate a successful monitoring of the localized aflatoxin contamination. In contrast to the destructive chemical analyses that measure the mean contamination of a certain number of maize kernels, we are able to measure the localized contamination in individual unprocessed food products. By monitoring the localized contamination level of the kernels, we allow to sort-out the maize kernels that contain a low mean contamination level but feature a small area with a high contamination level, which would not be detected by any type of chemical analyses. As a result, our developed optical detection methodology contributes to an improved food safety.

4. Extensibility of our research methodology to the detection of ochratoxin and zearalenone

Next to aflatoxins, also ochratoxin and zearalenone may be present in contaminated food products. Ochratoxins are mainly produced by the fungi *Penicillium verrucosum* and *Aspergillus ochraceus*, and occur most frequently in cereals, fruits and coffee beans. Cereal and cereal products are considered as the main contributors to the ochratoxin intake in Europe [27]. There exist five types of ochratoxins, of which only ochratoxin A and ochratoxin B occur naturally in food products. Particularly, ochratoxin A is considered as being the most common and most

toxic ochratoxin [28]. The European regulations limit the maximum allowed ochratoxin A concentration from 2 to 15 ppb, depending on the commodity [12]. Zearalenone, on the other hand, is a mycotoxin that can be produced by several fungi of the genus *Fusarium*, like *Fusarium graminearum*, *Fusarium culmorum* and *Fusarium cerealis* [29]. It mostly occurs in cereals as barley, oats, wheat, rice and maize. The European limitation on the zearalenone concentration ranges between 20 and 400 ppb [12].

In this section, we investigate the fluorescence characteristics of ochratoxin and zearalenone and discuss the applicability of our developed measurement methodology onto these toxins. Specifically, we performed measurements on pure ochratoxin A and zearalenone powder, purchased from Sigma-Aldrich.

4.1. Ochratoxin A detection

Ochratoxin A shows theoretically a strong absorbance in-between 200 and 275 nm and around 335 nm, while its theoretical fluorescence emission wavelength is situated around 475 nm (**Figure 3(b)**). The chemical analyses of ochratoxin A by using liquid chromatography in combination with fluorescence detection is widely discussed in literature [30–33]. During the execution of the fluorescence analysis, excitation wavelengths of 330, 332, 333 and 390 nm are commonly used, while the fluorescent detection occurs at 440, 460 and 476 nm.

Based on the absorbance spectrum of ochratoxin, while keeping in mind the wavelengths that are available with our fluorescence measurement configuration, we excite the ochratoxin A powder with 244, 250, 260, 356, 365, 375 and 395 nm during the OPIF measurements (**Figure 15**). The 244, 250 and 260 nm wavelengths are generated with the third-harmonic-generating crystal, while the 356, 365, 375 and 395 nm wavelengths are generated by the second-harmonic-generating crystal. To be able to compare the captured fluorescence intensities, we rescaled the fluorescence spectra to an excitation power density of 1 mW/mm^2 for all excitation wavelengths (illumination powers used during the measurements varied between 60 and 450 mW, depending on the excitation wavelength). For all excitation wavelengths, the measured fluorescence spectra indicate a maximum around 480 nm. Furthermore, the highest fluorescence intensity is obtained after excitation with 356 nm. In correspondence with the theoretical absorbance spectrum, the fluorescence intensity decreases when tuning the excitation wavelength from 244 to 260 nm and from 356 to 395 nm.

To measure the TPIF spectrum of the ochratoxin A powder, we used an excitation wavelength of 710 nm (with an excitation power of 562 mW and an excitation spot diameter of 375 μm), since the OPIF measurements showed the strongest fluorescence intensities after excitation with 356 nm. The obtained TPIF spectrum occurs in the same wavelength region as the OPIF spectrum, with a maximum fluorescence intensity at 480 nm (**Figure 16(a)**). However, the TPIF intensity is 1000 times weaker than the OPIF intensity and shows a larger noise contribution. To experimentally validate that we are measuring the TPIF spectrum of ochratoxin A, the integrated fluorescence intensity, obtained by integrating the fluorescence spectrum between 400 and 600 nm, is studied as a function of the excitation power (**Figure 16(b)**). Similar as for

aflatoxin B1, the integrated fluorescence intensity shows a quadratic dependence on the excitation power, corresponding with the non-linear behaviour of two-photon absorption.
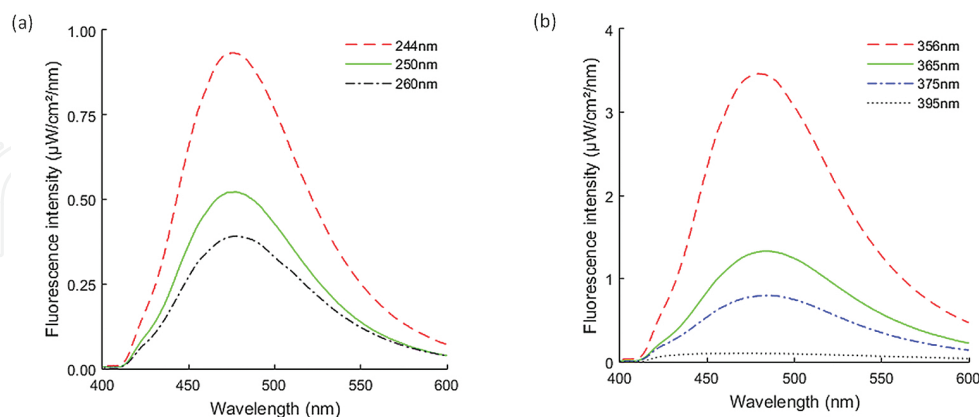

Figure 15. OPIF spectra of ochratoxin A: (a) spectra after excitation with 244, 250, 260 nm and (b) spectra after excitation with 356, 365, 375 and 395 nm.
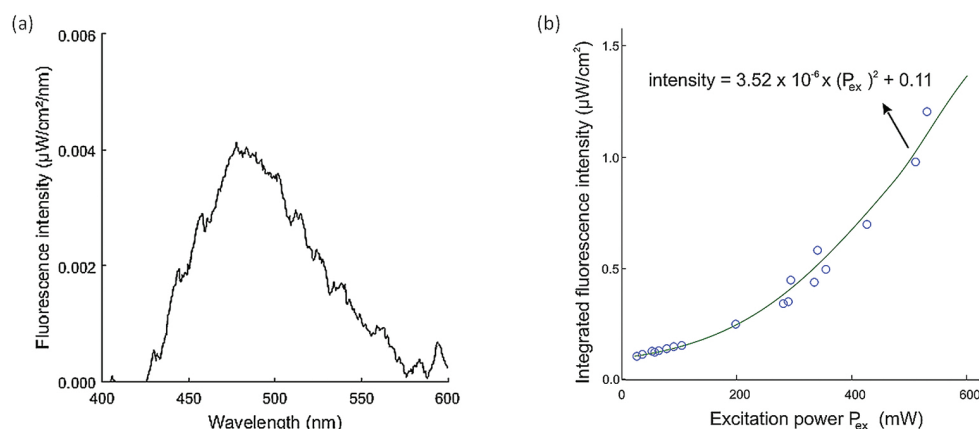

Figure 16. Study of TPIF of ochratoxin A: (a) TPIF spectrum after excitation with 710 nm and (b) quadratic relationship between the integrated fluorescence intensity and the excitation power, validating the two-photon absorption.

The fluorescence signal of the ochratoxin A powder shows a similar performance as the fluorescence of the aflatoxin B1 powder, but with excitation wavelengths of 356 and 710 nm during the OPIF and TPIF processes, respectively, instead of the 365 and 730 nm excitation wavelengths used during the aflatoxin characterization. As a result, the same research methodology as used during the aflatoxin detection on maize kernels can be applied to ochratoxin-contaminated food products.

4.2. Zearalenone detection

Zearalenone shows theoretically a strong absorbance between 200 and 350 nm and a maximum fluorescence intensity around 475 nm (**Figure 3(c)**). Similar to ochratoxin, the analysis of

zearalenone by using high-performance liquid chromatography in combination with fluorescence detection is widely discussed in literature [34–37]. During the execution of the fluorescence step, an excitation wavelength of 254, 274, 275 or 356 nm is often used, while the detection of the fluorescence signal occurs at 440, 446 or 470 nm. Applying the same measurement procedure to the zearalenone powder as to the ochratoxin A, we studied the zearalenone OPIF signal after excitation with 244, 250, 260, 365, 366, 375 and 395 nm (**Figure 17**). Particularly, to compare the fluorescence intensity for all excitation wavelengths, we present the fluorescence spectrum rescaled to an excitation power density of 1 mW/mm². The zearalenone fluorescence spectrum reaches its maximum between 425 and 500 nm. Its fluorescence spectrum shows a broader peak than the aflatoxin and ochratoxin fluorescence spectra. Furthermore, the zearalenone fluorescence emission shows approximately a 10 times weaker intensity than for ochratoxin A. However, similar to the ochratoxin A fluorescence, the largest fluorescence intensities are obtained after excitation with 244 and 356 nm.
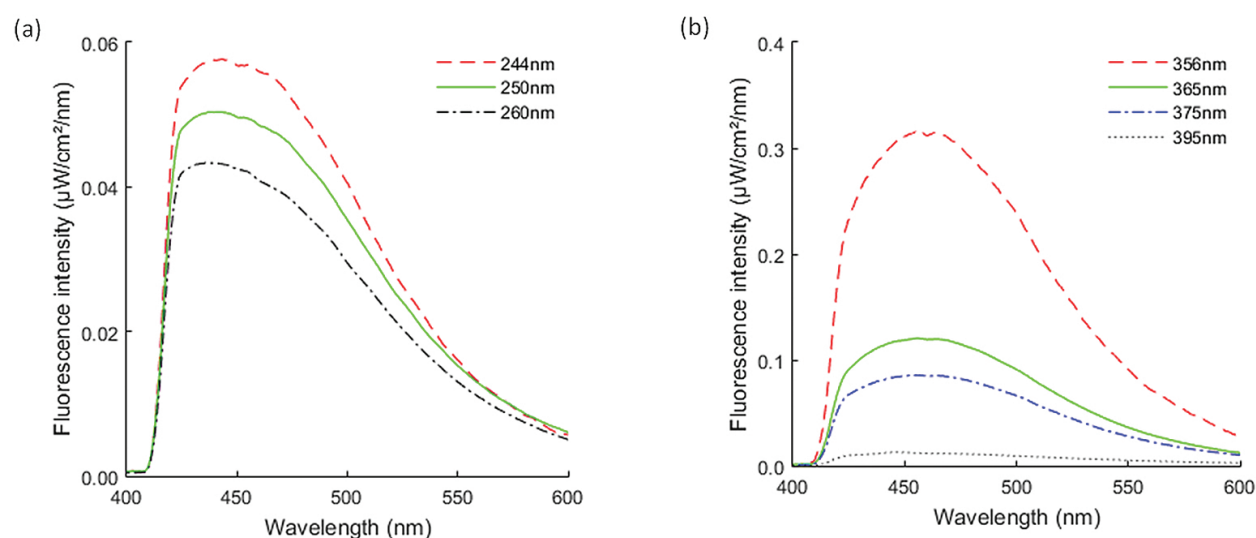

Figure 17. OPIF spectra of zearalenone: (a) spectra after excitation with 244, 250, 260 nm and (b) spectra after excitation with 356, 365, 375 and 395 nm.

To study the TPIF signal of zearalenone, we illuminated the zearalenone powder with 730, 750 and 780 nm, with a spot diameter of 231 μm and an excitation laser power of 1.10, 1.22 and 1.51 W, respectively (**Figure 18**). For all three excitation wavelengths, the measured spectra show two light signals: one at the excitation wavelength and one at half the excitation wavelength. The signal at the excitation wavelength represents the illumination laser light that reflects on the sample and reaches the spectrum analyser. Due to imperfections of the optical short-wave pass filter, small fractions of the high-power incident light are still able to reach the spectrum analyser. The signal at half the excitation wavelength, at 365, 375 and 385 nm for excitation with 730, 750 and 780 nm, respectively, represents SHG instead of TPIF. The absence of the TPIF signal can be explained by the study of the molecular structure of the zearalenone (**Figure 19**). Comparing the different molecular structures, zearalenone shows a significant different structure than aflatoxin B1 and ochratoxin A. Generally, molecules show a strong,

two-photon absorption if they feature a long conjugation system in combination with strong donor and acceptor groups, because this induces non-linearity in the system and increases the potential for charge transfer [19]. Consequently, the molecular structure of zearalenone favours SHG instead of TPIF. In comparison with TPIF, the SHG shows a smaller linewidth. During SHG, only one wavelength will be emitted for each illumination wavelength, because two incident photons will always recombine to the double energy. In contrast, during the TPIF process, different emission wavelengths are captured, since the relaxation of the exited electrons can start from different excited energy levels, dependant on their vibrational energy loss. Furthermore, the stronger the captured illumination signal, the weaker the generated SHG signal. When illuminating the sample, part of the excitation photons recombine to the SHG signal, while another part of the excitation signal reflects on the samples surface. The higher the amount of photons that recombine, the stronger the SHG signal and the lower the reflection on the sample.
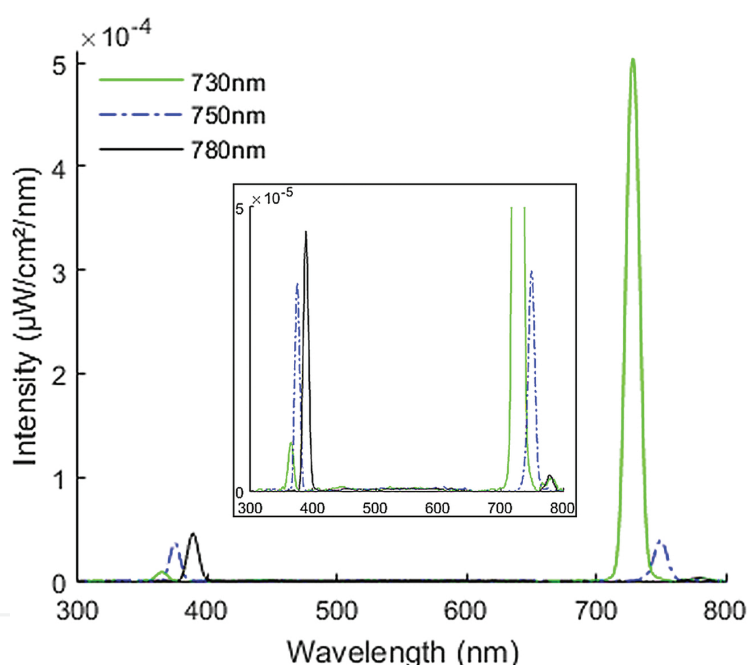

Figure 18. Second harmonic generation signal at 365, 375 and 385 nm, observed after illumination of the zearalenone powder with 730, 750 and 780 nm laser light, respectively. The inner graph presents a close-up on the weakest captured signals.
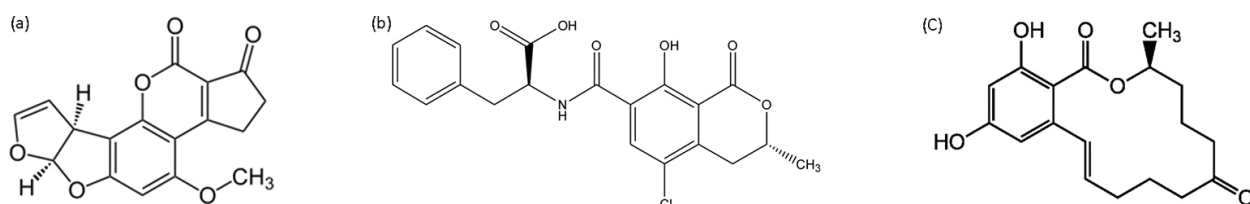

Figure 19. Chemical structure of (a) aflatoxin B1, (b) ochratoxin A and (c) zearalenone.

As a result, OPIF seems the most promising technique for the detection of zearalenone. In contrast to aflatoxin and ochratoxin, zearalenone does not show TPIF. Consequently, we consider TPIF as a less promising technique for the zearalenone detection. However, the influence of the zearalenone onto the intrinsic fluorescence of food products should be further investigated.

5. Conclusion

We successfully demonstrated the use of one- and two-photon-induced fluorescence spectroscopy for the detection of fluorescent mycotoxins in solid, unprocessed food products. First, we developed a sensitive measurement configuration able to study the localized one- and two-photon-induced fluorescence spectra of food products. Afterwards, as a case study, we investigated the detection of aflatoxin in individual maize kernels. We presented our research methodology, starting from the characterization of the aflatoxin fluorescence, to the measurement of the one- and two-photon-induced fluorescence spectra of the maize kernels and the development of a spectroscopic detection criterion. During both one- and two-photon-induced fluorescence processes, the fluorescence of the aflatoxin influenced the intensity and wavelength of the intrinsic fluorescence of the maize kernels. Based on the fluorescence spectrum between 400 and 550 nm, we defined an optical detection criterion, indicating a maximal contrast between the healthy and contaminated maize kernels for excitation with 365 and 780 nm, during one- and two-photon-induced fluorescence, respectively. Both one- and two-photon-induced fluorescence processes show a similar contrast. However, two-photon-induced fluorescence requires higher excitation power densities and a more sensitive detector than one-photon-induced fluorescence, but uses NIR laser wavelengths that are widely commercially available. Besides, in contrast to the chemical analyses that investigate the mean contamination of a batch of maize kernels, we successfully monitored the localized contamination level on the maize kernel surfaces. Both kernels containing a small area with a high contamination level and kernels containing a large region with a medium contamination level could be identified. Finally, we discussed the extensibility of our research methodology to the detection of ochratoxin A and zearalenone. Ochratoxin A showed a characteristic one- and two-photon-induced fluorescence signal, while for zearalenone only OPIF could be observed. Generally, we can conclude that we demonstrated the use of fluorescence spectroscopy as a valuable tool for the sensitive optical detection of fluorescent mycotoxins, paving the way for a non-destructive, real-time and high-sensitive industrial scanning-based detection.

Acknowledgements

Author details

Lien Smeesters[*], Wendy Meulebroeck and Hugo Thienpont

*Address all correspondence to: lsmeeste@b-phot.org

Department of Applied Physics and Photonics (TONA), Brussels Photonics Team (B-PHOT), Faculty of Engineering, Vrije Universiteit Brussel, Brussels, Belgium

References

[1] Jiskoot W, Hlady V, Naleway JJ, Herron JN. Physical Methods to Characterize Pharmaceutical Proteins [Internet]. Herron JN, Jiskoot W, Crommelin DJA, editors. Pharmaceutical Biotechnology. Boston, MA: Springer US; 1995. 1-63 p. (Pharmaceutical Biotechnology; vol. 7). Available from: http://link.springer.com/10.1007/978-1-4899-1079-0

[2] Hof M, Hutterer R, Fidler V. Fluorescence Spectroscopy in Biology. Vol. 3. Berlin Heidelberg: Springer; 2005. 131–286 p.

[3] Falla Sotelo F, Araujo Pantoja P, López-Gejo J, Le Roux GAC, Quina FH, Nascimento CAO. Application of Fluorescence Spectroscopy for Spectral Discrimination of Crude Oil Samples. Brazilian J Pet Gas. 2008;2(2):63–70.

[4] Wagnières GA, Star WM, Wilson BC. ln Vivo Fluorescence Spectroscopy and Imaging for Oncological Applications. Photochem Photobiol. 1998;68(5):603–32.

[5] Shahzad A, Köhler G, Knapp M, Gaubitzer E, Puchinger M, Edetsberger M. Emerging applications of fluorescence spectroscopy in medical microbiology field. J Transl Med. 2009;7:99.

[6] Meulebroeck W, Thienpont H. Optical detection techniques for laser sorting machines. In: SPIE Optical Sensing II. Strasbourg: SPIE; 2006. p. 1–12.

[7] Grzesiak MT, Rzepka A, Hura T, Grzesiak S, Hura K, Filek W, et al. Fluorescence excitation spectra of drought resistant and sensitive genotypes of triticale and maize. Photosynthetica. 2007;45(4):606–11.

[8] Nawrocka A, Lamorska J. Determination of Food Quality by Using Spectroscopic Methods. In: Grundas S, Stepniewski A, editors. Advances in Agrophysical Research. Rijeka: InTech; 2013. p. 347–68.

[9] Rasch C, Kumke M, Löhmannsröben HGG. Sensing of Mycotoxin Producing Fungi in the Processing of Grains. Food Bioprocess Technol [Internet]. Springer New York; 2010 Apr 29 [cited 2013 Jan 31];3(6):908–16. Available from: http://dx.doi.org/10.1007/s11947-010-0364-y

[10] Rasch C, Böttcher M, Kumke M. Determination of aflatoxin B1 in alcoholic beverages: Comparison of one- and two-photon-induced fluorescence. Anal Bioanal Chem. 2010;397(1):87–92.

[11] Hruska Z, Yao H, Kincaid R, Darlington D, Brown RL, Bhatnagar D, et al. Fluorescence imaging spectroscopy (FIS) for comparing spectra from corn ears naturally and artificially infected with aflatoxin producing fungus. J Food Sci. 2013;78(8).

[12] Romer Labs. Mycotoxin regulations [Internet]. 2012. p. 1–5. Available from: http://www.romerlabs.com/en/knowledge/mycotoxin-regulations/regulations-usa/

[13] European Commission. Commission regulation (EC) No 1881/2006 setting maximum levels for certain contaminants in foodstuffs. Official Journal of the European Union. Brussels; 2006 Dec.

[14] Lakowicz JR. Principles of Fluorescence Spectroscopy. Third Edit. New York: Springer Science + Business Media; 2006. 607-613 p.

[15] Kaiser W, Garrett CGB. Two-Photon Excitation in Ca:F2 Eu2+. Phys Rev Lett. 1961;7(6):229–31.

[16] Benninger RKP, Piston DW. Two-Photon Excitation Microscopy for the Study of Living Cells and Tissues. In: Current protocols in cell biology. Canada: John Wiley & Sons, Inc.; 2013. p. 4.11.1–4.11.24.

[17] Mulligan S, MacVicar B. Two-photon fluorescence microscopy: basic principles, advantages and risks. Mod Res Educ Top Microsc [Internet]. 2007;881–8. Available from: http://formatex.org/microscopy3/pdf/pp881-889.pdf

[18] Svoboda K, Yasuda R. Principles of Two-Photon Excitation Microscopy and Its Applications to Neuroscience. Neuron. 2006;50(6):823–39.

[19] Pawlicki M, Collins HA, Denning RG, Anderson HL. Two-photon absorption and the design of two-photon dyes. Angew Chemie–Int Ed. 2009;48(18):3244–66.

[20] Krueger A. MULTIPHOTON MICROSCOPY?: Turnkey femtosecond lasers fuel growth of multiphoton imaging. LaserFocusWorld. 2010;46(10):1–7.

[21] Avantes. Irradiance. In: AvaSoft for AvaSpec-USB2 User's Manual. Avantes; 2012. p. 63–4.

[22] Held P. Quantitation of Peptides and Amino Acids with a Synergy™ HT using UV Fluorescence. BioTek Instruments. 2006. p. 1–8.

[23] Smeesters L, Meulebroeck W, Raeymaekers S, Thienpont H. The use of one- and two-photon induced fluorescence spectroscopy for the optical characterization of carcinogenic aflatoxins. In: SPIE Ultrafast Nonlinear Imaging and Spectroscopy II [Internet]. San Diego: SPIE; 2014. p. 1–11. Available from: http://proceedings.spiedigitallibrary.org/proceeding.aspx?doi=10.1117/12.2061314

[24] ToxiMet. ToxiMet Advanced mycotoxin testing system [Internet]. 2014. Available from: http://www.toximet.com/technology/

[25] Downie NM, Health RW. Basic statistical methods. New York Harper; 1970. chapter 12.

[26] Smeesters L, Meulebroeck W, Raeymaekers S, Thienpont H. One- and two-photon induced fluorescence spectroscopy enabling the detection of localized aflatoxin contamination in individual maize kernels. In: Proc SPIE Optical Sensing and Detection IV. Brussels: SPIE; 2016. p. 98990X – 1–98990X – 15.

[27] Veterinary and Agrochemical Research Centre. Toxins and natural compounds: Ochratoxine (OTA) [Internet]. 2016 [cited 2016 Feb 27]. p. 2–4. Available from: http://coda-cerva.be/index.php?option=com_content&view=article&id=134&Itemid=293&lang=en

[28] Lawley R. Ochratoxins [Internet]. Food Safety Watch. Food Safety Watch; 2013 [cited 2016 Feb 21]. Available from: http://www.foodsafetywatch.org/factsheets/ochratoxins/

[29] Veterinary and Agrochemical Reseach Centre. Toxins and natural compounds: Zearalenone (ZEA) [Internet]. 2016 [cited 2016 Feb 27]. Available from: http://coda-cerva.be/index.php?option=com_content&view=article&id=136&Itemid=294&lang=en

[30] Studer-Rohr I, Dietrich DR, Schlatter J, Schlatter C. The occurrence of ochratoxin A in coffee. Food Chem Toxicol [Internet]. 1995;33(5):341–55. Available from: www.sciencedirect.com/science/article/B6T6P-3YKM35C-2D/1/bebc42a7963ba82d27f46fe1d7d4d201

[31] Lin L, Chen P, Fu Y, Shih DY. Ochratoxin A Contamination in Coffees , Cereals , Red Wines and Beers in Taiwan. J Food Drug Anal. 2005;13(1):84–92.

[32] Batista LR, Chalfoun SM, Silva CF, Cirillo M, Varga EA, Schwan RF. Ochratoxin A in coffee beans (Coffea arabica L.) processed by dry and wet methods. Food Control [Internet]. Elsevier Ltd; 2009 Sep [cited 2013 Jan 31];20(9):784–90. Available from: http://linkinghub.elsevier.com/retrieve/pii/S0956713508002818

[33] Cox KL. Analysis of Ochratoxin A Using the Hitachi LaChromUltra HPLC System with Fluorescence Detection. Californië: Hitachi; 2010.

[34] Arranz I, Mischke C, Stroka J, Sizoo E, van Egmond H, Neugebauer M. Liquid chromatographic method for the quantification of zearalenone in baby food and animal feed: interlaboratory study. J AOAC Int. 2007;90(6):1598–609.

[35] Diebold GJ, Karny N, Zare RN. Determination of zearalenone in corn by laser fluorimetry. Anal Chem. 1979;51(1):67–9.

[36] Huang ZB, Xu Y, Li LS, Li YP, Zhang H, He QH. Development of an immunochromatographic strip test for the rapid simultaneous detection of deoxynivalenol and zearalenone in wheat and maize. Food Control [Internet]. Elsevier Ltd; 2012;28(1):7–12. Available from: http://dx.doi.org/10.1016/j.foodcont.2012.04.035

[37] Pleadin J, Sokolović M, Perši N, Zadravec M, Jaki V, Vulić A. Contamination of maize with deoxynivalenol and zearalenone in Croatia. Food Control. 2012;28(1):94–8.